Effect of substitution of Y on the structural, magnetic, and thermal properties of hexagonal $DyMnO_3$ single crystals

Harikrishnan S. Nair,[1,2,*] C. M. N. Kumar,[1] H. L. Bhat,[2,3] Suja Elizabeth,[2] and Th. Brückel[1]

[1]*Institut für Festkörperforschung, Forschungszentrum Jülich, D-52425 Jülich, Germany*

[2]*Department of Physics, C.V. Raman Avenue, Indian Institute of Science, Bangalore 560012, India*

[3]*Centre for Soft Matter Research, Jalahalli, Bangalore 560013, India*

(Received 12 November 2010; revised manuscript received 8 January 2011; published 29 March 2011)

We investigate the structural, magnetic, and specific heat behavior of the hexagonal manganite $Dy_{0.5}Y_{0.5}MnO_3$ in order to understand the effect of dilution of Dy magnetism with nonmagnetic yttrium. In this compound, the triangular Mn lattice orders antiferromagnetic at $T_N^{Mn} \approx 68$ K observed experimentally in the derivative of magnetic susceptibility as well as in specific heat. In addition, a low-temperature peak at $T_N^{Dy} \sim 3$ K is observed in specific heat which is attributed to rare earth order. The T_N^{Mn} increases by 9 K compared to that of hexagonal (h)$DyMnO_3$ while T_N^{Dy} is unchanged. A change in slope of thermal evolution of lattice parameters is observed to occur at temperature close to T_N^{Mn}. This hints at strong magnetoelastic coupling in this geometric multiferroic. In magnetization measurements, steplike features are observed when the magnetic field is applied along the c axis which shift to higher fields with temperature and vanish completely above 40 K. The presence of different magnetic phases at low temperature and strong magnetoelastic effects can lead to such field-induced transitions which resemble *metamagnetic* transitions. This indicates the possibility of strong field-induced effects in dielectric properties of this material, which is unexplored to date.

DOI: 10.1103/PhysRevB.83.104424 PACS number(s): 75.85.+t, 75.47.Lx

I. INTRODUCTION

Recent findings of vortices in hexagonal $YMnO_3$ confirm the formation of composite multiferroic domain walls and reaffirm the geometric nature of polarization in hexagonal(h) $RMnO_3$ (R = rare earth).[1,2] These reports have motivated the search for new hexagonal $RMnO_3$ and an improved understanding of bulk properties. The (h)$RMnO_3$ multiferroics are different from their perovskite counterparts due to two main reasons: First, the origin of polarization is structural rather than magnetic.[3] Second, they possess multiple magnetic sublattices for the rare earth ion and a 120° triangular lattice for Mn.[4] These two reasons suggest the possibility of enhancing the multiferroicity in hexagonal systems by perturbing the asymmetric coordination of rare earth through structural tuning as well as by relieving the magnetic frustration in the Mn sublattice. The (h)$RMnO_3$ are ferroelectric (FE) below $T_c \approx 900$ K[5] and antiferromagnetic (AFM) below $T_N \approx 80$ K. Complex magnetic phases pertaining to the different sublattices are theoretically predicted in hexagonal manganites[6] and are experimentally observed as field-induced modification of the magnetic structure.[7] Reentrant magnetic phases have been observed in $HoMnO_3$[8] which were attributed to the indirect coupling between the FE and AFM orders arising from domain wall effects. In the case of hexagonal (Ho, Yb, Er)MnO_3 a magnetic phase due to rare earth was detected at low temperature which transformed into two phases with the application of the magnetic field.[9] In addition to different magnetic phases, giant changes in atomic positions in zero and under applied magnetic field were observed in (h)$RMnO_3$.[10,11] For example, in dielectric studies of $HoMnO_3$, anomalies in the c-axis length were observed in applied magnetic field indicating strong magnetoelastic coupling.[12]

The bulk magnetic properties[13] and magnetic structures of the end compounds (h)$DyMnO_3$ and $YMnO_3$ are studied[4,14] and in $YMnO_3$, the Mn spins adopt a triangular AFM magnetic structure Γ_1 where the spins of the layers $z = 0$ and $z = 1/2$ are antiferromagnetically coupled.[14] However, Dy^{3+} moments adopt a Γ_3 structure where they align in the hexagonal c direction in the temperature range $8 \leqslant T \leqslant 68$ K. Below 8 K, the magnetic structure changes to Γ_2 representation with a ferrimagnetic alignment of moments.[4] Solid solutions of hexagonal manganites with different magnetic phases have been studied as $Ho_{1-x}Y_xMnO_3$[15] and $Er_{1-x}Y_xMnO_3$.[16] In both cases, existence of mixed magnetic phases were evidenced and with Y substitution, a reduction in magnetic frustration in the Mn lattice was observed. In the present study we dilute the influence of rare earth magnetism in (h)$DyMnO_3$ with Y substitution to see the effects of coupling between R and Mn lattices without directly disturbing the Mn sublattice.

II. EXPERIMENTAL

Polycrystalline $Dy_{0.5}Y_{0.5}MnO_3$ (DYMO50) was prepared by solid-state reaction of Dy_2O_3 (4N), MnO_2(4N), and Y_2O_3(4N) in stoichiometric ratio. After confirming the phase purity by powder x-ray diffractograms, single crystals were grown by float-zone technique using an image furnace (FZ-T-10000-H-VI-VP). Successful growth experiments resulted in crystals of dimension 6-mm diameter and 60-mm length. Quality of the grown crystals was ascertained through Laue photographs which showed that the hexagonal c axis is almost perpendicular to the growth axis. Powder x-ray diffractograms (PXD) of crushed single crystal samples were obtained in the temperature range 10–300 K, using a Huber instrument in transmission Guinier geometry. Rietveld analysis[17] of the powder data was performed using the FULLPROF suite of programs.[18] Magnetic and thermal measurements were performed using a commercial PPMS and MPMS (both Quantum Design).

III. CRYSTAL STRUCTURE

The PXD patterns obtained on DYMO50 (at 300 K) along with the results of the Rietveld analysis are presented in Fig. 1(a). The refinement suggests a space group $P6_3cm$ the same as $(h)DyMnO_3$.[13] The refined lattice parameters are $a = 6.161(1)$ (Å), and $c = 11.446(2)$ (Å). The quality of fit is indicated by $\chi^2 = 3.24$. No structural transitions were observed in the range 10–300 K. The temperature variation of unit cell volume is shown in Fig. 1(b) where the insets (1) and (2) show, respectively, the variation of a and c with temperature. A change of slope near 70 K is clearly visible in these plots. A similar temperature evolution of cell volume and lattice constants was observed in $(h)YMnO_3$ where atomic positions, bond distances, and bond angles showed anomalies at T_N^{Mn}, thus, indicating strong magnetoelastic coupling.[10,11] The unit cell volume of DYMO50 was modeled following the Grüneisen approximation[19] using the expression, $V(T) = \gamma \; U(T)/K_0 + V_0$; $U(T) = 9 \; Nk_BT(T/\Theta_D)^3 \int_0^{\Theta_D/T} x^3/(e^x - 1)dx$. Here, γ is the Grüneisen parameter, K_0 is the incompressibility, and V_0 is the volume at $T = 0$ K and Θ_D is the Debye temperature. The value of Θ_D obtained from the fit was 441.23(21.6) K and $V_0 = 373.85$ (Å). The result of the fit is shown as a solid line in Fig. 1(b). Note that the fit line deviates from the data at ~75 K where the lattice constants and the volume also reflects a marked change. This is inferred as a clear indication of magnetoelastic or magnetovolume effects present in this system.

IV. MAGNETIZATION

Magnetization, M(T), in field-cooled (FC) and zero field-cooled (ZFC) cycles, shown in the main panel of Fig. 2, displays a monotonic increase with decreasing temperature. However, two anomalies are observed in the derivative of inverse susceptibility $[d(1/\chi)/dT] \parallel$ to the c axis presented in the inset (a) of Fig. 2. The anomaly at $T_N^{Mn} \sim 68$ K relates to the Mn ordering and is not observed in $(d(1/\chi)/dT)$ perpendicular to c. Another anomaly is observed at 10 K which could arise from a reorientation process in the Mn or rare earth spins. Mn reorientation below T_N^{Mn} has been reported for hexagonal $HoMnO_3$ resulting from the change in orientation of Mn spins in the basal plane.[20] The rare earth order at $T_N^{Dy} \sim 3$ K (observed in specific heat, discussed later) is not observed in the $\chi(T)$ as the lowest measurement temperature was 4.2 K in this case. The inverse susceptibility plots $\parallel$ and $\perp$ to c along with CW fits are shown in the inset (b) of Fig. 2. Deviation from linearity is observed below 100 K and the fit results in a Curie-Weiss (CW) temperature, $\Theta_{CW} = -37(4)K \parallel c$ and $-29(2)K \perp c$. This signifies predominant antiferromagnetic correlations and the anisotropic character of interactions between the Mn spins in the ab plane separated along the c axis by a layer of R. The effective magnetic moment obtained from the fit, $\mu_{exp} = 8.15(5)\ \mu_B$, is lower than the theoretical value $\mu_{calc} = 9.70\ \mu_B$ obtained assuming spin-orbit coupling for the rare earth ion. In the case of $YMnO_3$, a clear deviation from the CW description was observed at 250 K itself, signifying the presence of spin fluctuations related to a two-dimensional (2D) short-range type.[21] Similarly, in the present frustrated magnet also, a CW description may not be the accurate one.

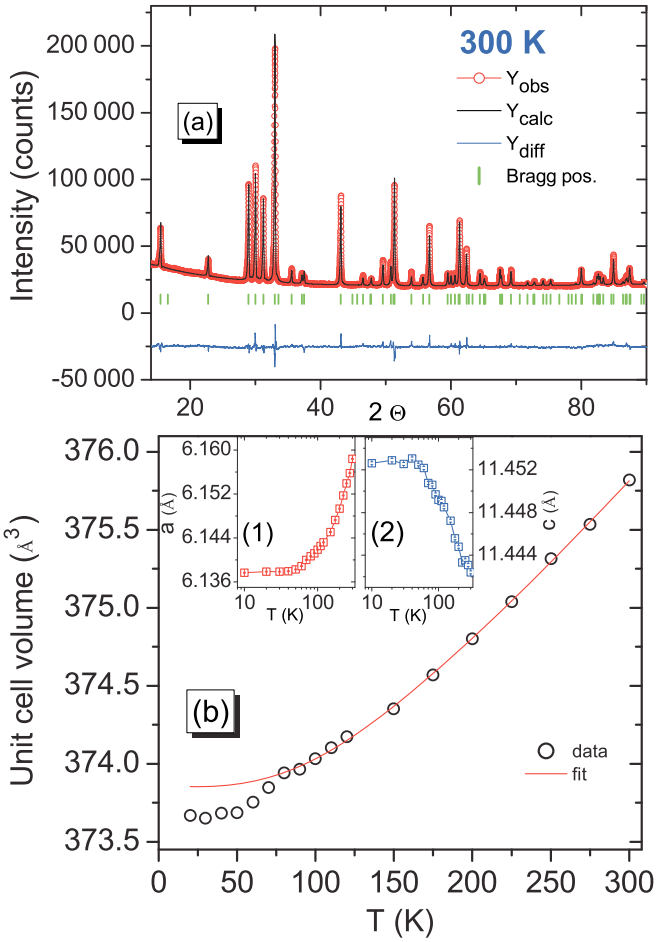

FIG. 1. (Color online) (a) The powder x-ray diffraction pattern obtained on crushed single crystals of $Dy_{0.5}Y_{0.5}MnO_3$ at 300 K. The results of Rietveld analysis are shown. (b) The variation of unit cell volume with temperature. The solid line is the fit according to Grüneisen approximation. Temperature evolution of a and c are shown in insets (1) and (2), respectively.

The observed linearity of inverse susceptibility still has a major contribution from the paramagnetic susceptibility of Dy. Hence, the deviation of the experimentally observed effective moment indicates the presence of short-range spin fluctuations above T_N^{Mn} and the inadequacy of CW law to describe complex magnetic systems. Detailed neutron scattering experiments can reveal the role of spin fluctuations above T_N^{Mn}, as done in the case of $YMnO_3$.[22] Electron paramagnetic studies on the parent hexagonal $DyMnO_3$ has shown that the spin fluctuations persist even above the T_N^{Mn}.[23] The frustration parameter calculated as $f = \Theta_{CW}/T_N = 1.53$ for $(h)DyMnO_3$ reduces to 0.54 for DYMO. Note that f in the present case is a very small value, lower than 1. We want to point out that the ratio Θ_{CW}/T_N is not a rigorous measure of the extent of magnetic frustration of the system. This has been emphasized in detailed magnetic structure studies of spinel MnO_2 and pyrochlore $Y_2Mn_2O_7$, both of which are frustrated magnets.[24] Following the CW analysis, they observe an f value of 3 which is not high enough to represent a frustrated magnet. However, a careful magnetic structure evaluation establishes the importance of magnetic frustration and the fact that a high value of Θ_{CW}/T_N

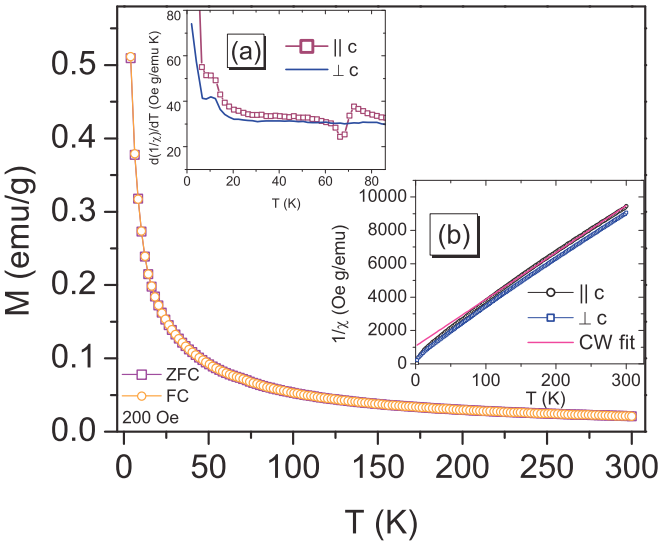

FIG. 2. (Color online) The FC/ZFC cycles of magnetization for an applied field of 200 Oe parallel to the c axis. (a) Derivative of $1/\chi$ $\parallel c$ showing anomalies at 68 K and at 10 K. (b) Inverse susceptibility $\parallel$ and $\perp$ to c. Curie-Weiss (CW) fit in one case ($\parallel c$) is shown. The fit deviates markedly below 100 K.

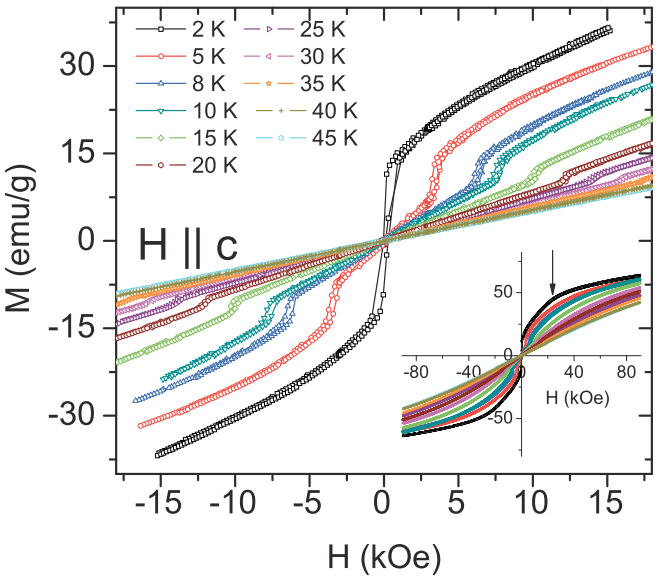

FIG. 3. (Color online) The M(H) plots of $Dy_{0.5}Y_{0.5}MnO_3$ at various temperatures up to 45 K measured with H $\parallel$ to c. Clear steplike features are observed. The steps vanish above 45 K. The inset shows the measurement in full field range.

is not a necessary condition for frustration. Moreover, the estimation of Θ_{CW} from the CW fit for DYMO50 can be inaccurate as mentioned above. Following[24] we believe that a real picture of magnetic frustration can be captured through neutron scattering experiments.

Isothermal magnetization measurements with applied field, H $\parallel$ to the c axis measured up to 9 T are presented in the inset and magnified in the main panel of Fig. 3. The M(H) curves showed clear and symmetric steps accompanied by hysteresis. In addition, the clear change of slope is observed at 20 kOe in the magnetization $\parallel$ to c at 2 K, as indicated by the arrow in the inset of Fig. 3. The critical field, H_c, at which these steps occur shifts to higher values with increasing temperature and eventually vanishes above 40 K. This is clear in the derivative plot, dM/dH in Fig. 4(a). A comparison of the M(H) of $(h)DyMnO_3$ and DYMO50 in Fig. 4(b) shows that the magnetization of the latter has reduced to almost half the value of $(h)DyMnO_3$ as a result of Y dilution. A reduction in the height of the steps also is apparent. Extrapolation of the magnetization data at high fields toward abscissa indicates a value less than 1 μ_B for DYMO50, which is lower than that for $(h)DyMnO_3$. This might be an indication that the Dy moments adopt a ferrimagnetic Γ_2 alignment same as in $(h)DyMnO_3$. The steplike features in M(H) have been previously observed in $(h)DyMnO_3$[25], being prominent below 45 K. In $(h)RMnO_3$, numerical calculations based on group theory and Landau theory showed that the coupling between various order parameters leads to a complex magnetic field—temperature phase diagram.[6] In this respect, we recall the case of $(h)HoMnO_3$ where five different magnetic phases were identified.[26] Anomalies in the thermal expansivities at the antiferromagnetic and the spin-rotation transition temperature and a negative c-axis expansivity were observed in this compound.[27] Detailed study of dielectric constant of $HoMnO_3$ at low temperature under external magnetic field revealed a complex phase diagram with reentrant phases, thermal and field hysteresis, and anomalies in c axis at low temperature with applied magnetic field.[12] The temperature variation of the critical field at which the steps occur, H_c, is shown in Fig. 4(c). Notably, the steplike features in M(H) are absent in magnetization measurements performed perpendicular to the c axis [Fig. 4(d)] which is suggestive of the highly anisotropic nature of the magnetic interactions.

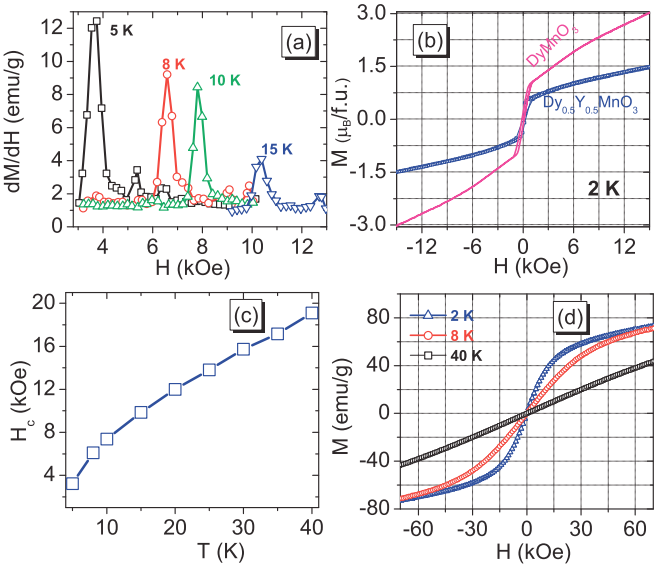

FIG. 4. (Color online) (a) The plot of dM/dH versus H along c at various temperatures shows the peak shifting to higher fields with temperature. (b) A comparison of M(H) plots of $Dy_{0.5}Y_{0.5}MnO_3$ and $(h)DyMnO_3$ at 2 K. (c) The variation of H_c with temperature. (d) M(H) curves recorded with H $\perp$ to c at 2, 8, and 40 K. The steplike transitions are absent in this case.

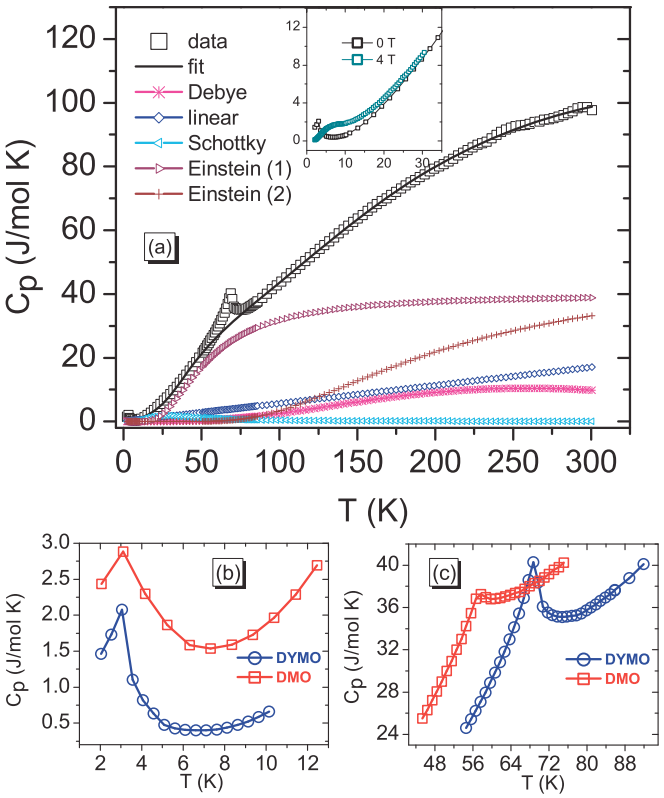

FIG. 5. (Color online) (a) The specific heat of $Dy_{0.5}Y_{0.5}MnO_3$ plotted along with the fit results. Different contributions to the total C_p are also shown. Inset of (a) shows the effect of magnetic field applied along c, in suppressing the low-temperature magnetic peak. (b) Shows the low-temperature peak, which shows no change with Y dilution. (c) Shows that T_N^{Mn} is shifted by 10 K with Y dilution of (h)$DyMnO_3$ (DMO).

The nature of magnetization curves close to $H = 0$ resembles that of an antiferromagnet. As the temperature is increased, the steplike features with hysteresis become less pronounced. This is suggestive of a ferrimagnetic state due to the alignment of Dy moments similar to that observed in (h)$DyMnO_3$.[25] The magnetic steps as well as the derivative dM/dH versus H is similar to the bahavior of *metamagnetic* systems like $Na_{0.85}CoO_2$.[28] In the present case, the steplike features are attributed to phase transitions between different magnetic phases possessed by the Mn lattice and the R lattice.[6]

V. SPECIFIC HEAT

The observed specific heat, C_p, of DYMO50 is presented in Fig. 5 as black squares. The peak at $T_N^{Mn} \sim 68$ K relates to Mn order while $T_N^{Dy} \sim 3$ K is the rare earth ordering temperature (the feature observed at ~250 K is a measurement artifact). In order to clearly see the effects of Y substitution on these transitions, the specific heat of (h)$DyMnO_3$ is plotted along with C_p of DYMO50 in Figs. 5(b) and 5(c). Two differences are evident. First, with Y dilution, the magnitude of C_p decreases. Second, T_N^{Mn} is increased by ≈10 K. However, the position of the low-temperature peak, T_N^{Dy}, is not altered in DYMO and occurs at 2.7 K. The inset of Fig. 5(a) shows the effect of the magnetic field on the low-temperature part of C_p.

In order to analyze the thermal properties quantitatively, the total specific heat was modeled by assuming contributions from lattice (C_{lattice}), electrons(C_{linear}), and Schottky levels (C_{Schottky}). The C_{lattice} is assumed to consist of contributions from a Debye term (C_{Debye}) and an Einstein term (C_{Einstein}).

$$C_p = C_{\text{linear}} + C_{\text{lattice}} + C_{\text{Schottky}},$$
$$C_{\text{lattice}} = C_{\text{Debye}} + C_{\text{Einstein}},$$

where

$$C_{\text{linear}} = \gamma T,$$
$$C_{\text{Debye}} = 9rR/x_D^3 \int_0^{x_D} x_D^4 e^{x_D}/(e^{x_D}-1)^2 dx_D,$$
$$C_{\text{Einstein}} = 3rR \sum_i a_i \left[x_i^2 e^{x_i}/(e^{x_i}-1)^2\right],$$
$$C_{\text{Schottky}} = A(1-x)R \sum_i w_i \frac{\left(\frac{\Delta_i}{k_B T}\right)^2 \exp\left(\frac{\Delta_i}{k_B T}\right)}{\left[1+\exp\left(\frac{\Delta_i}{k_B T}\right)\right]^2}.$$

Here, $x_D = \hbar\omega_D/k_B T$ and $x_i = \hbar\omega_E/k_B T_i$, N is the number of atoms in unit cell, A specifies the percentage of Dy involved in the Schottky anomaly, x is the fraction of Y, and Δ_i is the crystal field energy level. Based on the scattering results on (h)$DyMnO_3$[4], we fixed the value of Δ_i near 5.8 meV (~68 K). Later, Δ_i was varied as a free parameter in the least squares. The value of γ obtained from the fit is 0.056 J/mol K^2, which is small compared to the case of $Ho_{1-x}Y_xMnO_3$[15] or $RMn_{1-x}Ga_xO_3$[29] where a value of 0.19 was reported. The presence of a linear term is attributed to the high degeneracy of disordered rare earth spins.[15,30] The values of Θ_D and two Einstein temperatures, $\Theta_{E1,E2}$, obtained from the fit are 873(11), 635(24), and 166(12) K, respectively. The value of Δ_i obtained from the fit was 60(5) K, which is close to the result from (h)$DyMnO_3$. In order to analyze the low-temperature specific heat, the data were fitted for $T \leqslant 45$ K considering contributions from the lattice, a linear term, and Schottky levels. Results of the low-temperature analysis for 0 and 4 T are presented in Figs. 6(a) and 6(b), respectively. An estimate of $\Theta_D = 244(15)$ K was made from the low-temperature fit for 0 T data. This value is close to that obtained from the Grüneisen approximation of unit cell volume. A value of 75(6) K (6.4 meV) was obtained for Δ_i in the zero field and 80(8) K with the application of 4 T. The low-temperature fit of C_p in a short temperature range gives a higher value of Δ_i than that obtained from the full-temperature fit shown above. It is noted that the specific heat fits do not include a valid spin-wave term. This might affect the values of the low-temperature analysis. In the present case, it was difficult to accommodate a spin-wave term in the low-temperature fits. The accurate value of Δ_i cannot be commented upon as the crystal field level schemes of Dy^{3+} is not clearly understood.

VI. DISCUSSION

To summarize, structural characterization of $Dy_{0.5}Y_{0.5}MnO_3$ confirms the $P6_3cm$ hexagonal symmetry common to hexagonal $RMnO_3$ multiferroics. Interestingly, a change of slope in thermal evolution of lattice constants occurs

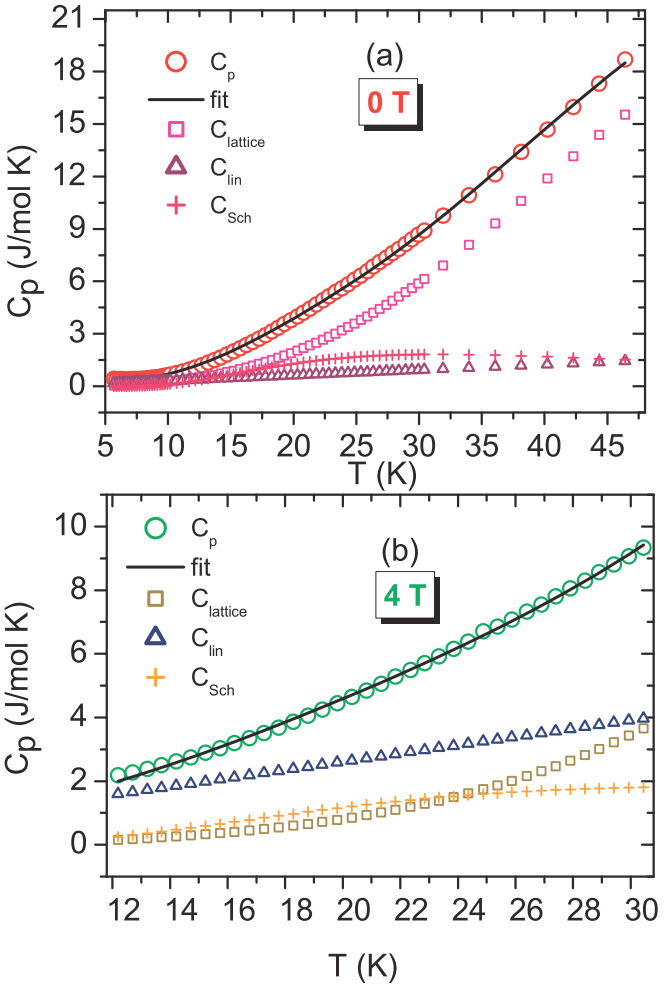

FIG. 6. (Color online) The low-temperature specific heat along with the fit results for $Dy_{0.5}Y_{0.5}MnO_3$ in (a) 0 T and (b) 4 T.

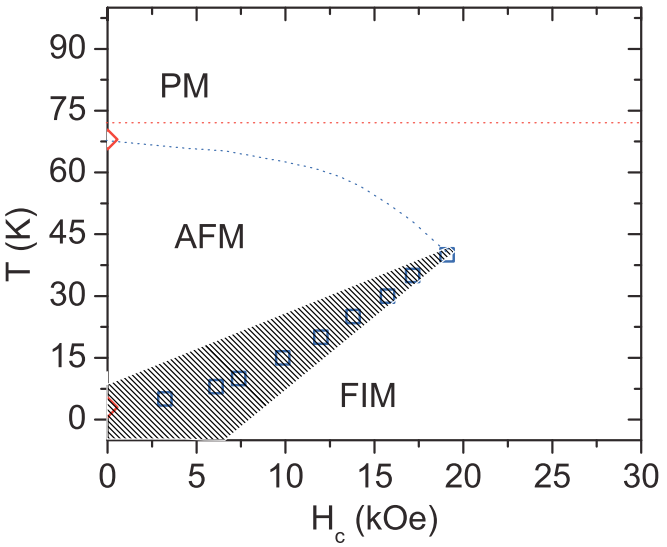

FIG. 7. (Color online) A tentative H-T phase diagram of $Dy_{0.5}Y_{0.5}MnO_3$. The red open diamonds are determined from specific heat measurements, the blue open squares from magnetization measurements. The shaded region represents hysteresis as observed in the magnetization. The abbreviations are as follows: paramagnetic (PM), antiferromagnetic (AFM), and ferrimagnetic (FIM).

at the magnetic transition temperature T_N^{Mn}. This signals strong magnetoelastic coupling which is also supported by the direct observation of *colossal* atomic displacements at the magnetic transitions under zero and applied magnetic fields in $YMnO_3$ through scattering experiments.[10,11] Steplike features observed in magnetization below 45 K indicate possible multiple magnetic phases or orientation transitions of Mn/Dy spins. Similar ferrimagnetic order as in the end compound $(h)DyMnO_3$ can lead to such features.[25] In this respect, neutron scattering studies aimed at elucidating the magnetic structure are necessary. Nonmagnetic Y dilution at the Dy site is likely to mitigate the difficulties arising from the strong absorption cross section of Dy. From the specific heat measurements it is found that the Y dilution enhances the T_N^{Mn} by 10 K where as T_N^{Dy} remains unaffected. This increase of T_N^{Mn} with nonmagnetic substitution at the Dy site is an indication of the complex magnetic couplings present in this system which certainly go beyond a simple mean-field explanation. An earlier neutron scattering study on $YMnO_3$ has shown that the interlayer magnetic coupling through the exchange path $Mn - O1 - O2 - Mn$ is weaker than the intralayer coupling along $Mn - O3 - Mn$ or $Mn - O4 - Mn$ (here, $O1$, $O2$ are apical oxygens and $O3$, $O4$ are oxygens in the basal plane of the MnO_5 bipyramid).[21] Insertion of nonmagnetic Y atoms between the layers of Mn bipyramids will only weaken the interlayer exchange further. The fact that the T_N^{Mn} has increased indicates the importance of the intralayer coupling between Mn in the basal plane. Furthermore, a plot of ionic radius of the rare earth ion (r_R) versus T_N^{Mn} of various hexagonal $RMnO_3$ shows that the T_N^{Mn} decreases linearly as r_R increases. On such a curve, the projected position of DYMO50 lies close to 70 K highlighting the role of r_R in the magnetism of these materials. It is also worth pointing out that the end-member $YMnO_3$ is reported to possess a T_N^{Mn} in the range of 70–75 K.[22,31,32] However, surprising observation is that even after 50% dilution of the magnetic lattice, T_N^{Dy} remains unchanged. A valid explanation for this observation has to wait until a clear picture of magnetic structure in this material emerges. The determination of magnetic structure of Dy through neutrons is rendered difficult by the high absorption cross section. However, studies using resonant absorption of x rays are useful in this aspect.[4] It is worth pointing out that detailed neutron scattering and polarimetry experiments were carried out to address the problems in identifying different magnetic structures that give identical diffraction intensities of the end-compound $YMnO_3$.[33] It has been shown that $YMnO_3$ indeed has a symmetry lower than *6mm*. Furthermore, Y substitution in other hexagonal magnets like $HoMnO_3$ and $ErMnO_3$ has displayed the presence of mixed magnetic structures.[15,16] These studies indicate that the magnetic structure of DYMO50 might also be a complex one and would require a careful examination to understand the magnetic structure and phases.

It is interesting to note that the parent $DyMnO_3$ and the substituted compounds show different structural and magnetic behavior. Usual ceramic synthesis of $DyMnO_3$ results in the

orthorhombic $Pnma$ structure while, the hexagonal $P6_3cm$ variant is stabilized through special synthesis conditions.[13] Orthorhombic $DyMnO_3$ is a helical magnet which is multiferroic while the hexagonal one is a frustrated magnet. Chemical substitution of Sr^{2+} in $DyMnO_3$ (up to $x = 0.5$) retains the orthorhombic symmetry. Detailed investigations on $Dy_{0.5}Sr_{0.5}MnO_3$ revealed spin glasslike behavior.[13,23,34] Low concentration of Y^{3+} in $Dy_{1-x}Y_xMnO_3$ ($x \leqslant 0.1$) retains the orthorhombic $Pnma$ structure. For $0.2 \leqslant x \leqslant 0.4$ mixed phases are observed and for $x = 0.5$, hexagonal symmetry stabilizes with complex magnetic structure.

VII. CONCLUSIONS

Based on results of phase transition studies in zero and applied fields in different experiments, we constructed a tentative H-T phase diagram and it is presented in Fig. 7. Note that the general features of the phase diagram are in conformance with the theoretical predictions of a generic phase diagram of $(h)RMnO_3$.[6] The blue dotted line in the figure connects the data points and marks the boundary between different possible magnetic phases. The hysteresis observed at the magnetization steps are represented as a shaded region. In the paper by Munawar *et al.*,[6] different magnetic phases pertaining to the Mn and the R moments are designated as A_1, A_2, B_1, and B_2. Identification of these phases in $Dy_{0.5}Y_{0.5}MnO_3$ would pose a challenging task and remains to be completed with the aid of detailed scattering experiments. Orientation effects of Mn and/or Dy ions, magnetic frustration, and the magnetoelastic effects are expected to play an important role in this material. We conclude by observing that dielectric, thermal expansion, and neutron scattering experiments to probe the magnetoelastic coupling in this material at the magnetic transition might be highly rewarding.

ACKNOWLEDGMENTS

Financial support through FIST is acknowledged. The authors H.L.B. and S.E. wish to thank Department of Science and Technology, India for financial support. H.S.N. wishes to thank IFF, Jülich for financial support and hospitality. H.S.N. and C.M.N.K. wish to acknowledge M. Angst and S. Nandi for useful discussions. J. Perßon is thanked for help with orienting the crystals.

*hari@physics.iisc.ernet.in, krishnair1@gmail.com

[1] T. Choi, Y. Horibe, H. T. Yi, Y. J. Choi, W. Wu, and S.-W. Cheong, Nat. Mater. **9**, 253 (2010).
[2] M. Fiebig, Th. Lottermoser, D. Fröhlich, A. V. Goltsev, and R. V. Pisarev, Nature (London) **419**, 818 (2002).
[3] B. B. van Aken, T. T. M. Palstra, A. Filippetti, and N. A. Spaldin, Nat. Mater. **3**, 164 (2004).
[4] S. Nandi, A. Kreyssig, J. Q. Yan, M. D. Vannette, J. C. Lang, L. Tan, J. W. Kim, R. Prozorov, T. A. Lograsso, R. J. McQueeney *et al.*, Phys. Rev. B **78**, 075118 (2008).
[5] Th. Lonkai, D. G. Tomuta, U. Amann, J. Ihringer, R. W. A. Hendrikx, D. M. Többens, and J. A. Mydosh, Phys. Rev. B **69**, 134108 (2004).
[6] I. Munawar and S. H. Curnoe, J. Phys. Condens. Matter. **18**, 9575 (2006).
[7] M. Fiebig, D. Fröhlich, T. Lottermoser, and R. V. Pisarev, Phys. Rev. B **65**, 224421 (2002).
[8] B. Lorenz, A. P. Litvinchuk, M. M. Gospodinov, and C. W. Chu, Phys. Rev. Lett. **92**, 087204 (2004).
[9] H. Sugie, N. Iwata, and K. Kohn, J. Phys. Soc. Jpn. **71**, 1558 (2002).
[10] S. Lee, A. Pirogov, M. Kang, K.-H. Jang, M. Yonemura, T. Kamiyama, S.-W. Cheong, F. Gozzo, N. Shin, H. Kimura *et al.*, Nature (London) **451**, 805 (2008).
[11] A. K. Singh, S. Patnaik, S. D. Kaushik, and V. Siruguri, Phys. Rev. B **81**, 184406 (2010).
[12] F. Yen, C. R. dela Cruz, B. Lorenz, Y. Y. Sun, Y. Q. Wang, M. M. Gospodinov, and C. W. Chu, Phys. Rev. B **71**, 180407(R) (2005).
[13] S. Harikrishnan, S. Rößler, C. M. N. Kumar, H. L. Bhat, U. Rößler, S. Wirth, F. Steglich, and S. Elizabeth, J. Phys. Condens. Matter **21**, 096002 (2009).
[14] A. Muñoz, J. A. Alonso, M. J. Martínez-Lope, M. T. Casáis, J. L. Martínez, and M. T. Fernández-Diaz, Phys. Rev. B **62**, 9498 (2000).
[15] H. D. Zhou, J. Lu, R. Vasic, B. W. Vogt, J. A. Janik, J. S. Brooks, and C. R. Wiebe, Phys. Rev. B **75**, 132406 (2007).
[16] M. C. Sekhar, S. Lee, G. Choi, C. Lee, and J.-G. Park, Phys. Rev. B **72**, 14402 (2005).
[17] H. M. Rietveld, J. Appl. Cryst. **2**, 65 (1969).
[18] J. Rodriguez-Carvajal, Physica B **192**, 55 (1993).
[19] D. C. Wallace, *Thermodynamics of Crystals* (Dover, New York, 1998).
[20] A. Munoz, J. A. Alonso, M. J. Martinez-Lope, M. T. Casais, J. L. Martinez, and M. T. Fernandez-Diaz, Chem. Mater. **13**, 1497 (2001).
[21] Th. Lonkai, D. G. Tomuta, J.-U. Hoffmann, R. Schneider, D. Hohlwein, and J. Ihringer, Appl. Phys. **93**, 8191 (2003).
[22] J. Park, J.-G. Park, G. S. Jeon, H.-Y. Choi, C. Lee, W. Jo, R. Bewley, K. A. McEwen, and T. G. Perring, Phys. Rev. B **68**, 104426 (2003).
[23] S. Harikrishnan, C. M. N. Kumar, S. S. Rao, H. L. Bhat, S. V. Bhat, and Suja Elizabeth, J. App. Phys. **104**, 023902 (2008).
[24] J. E. Greedan, N. P. Raju, A. S. Wills, C. Morin, and S. M. Shaw, Chem. Mater. **10**, 3058 (1998).
[25] V. Yu. Ivanov, A. A. Mukhin, A. S. Prokhorov, A. M. Balbashov, and L. D. Iskhakova, Phys. Solid State **48**, 1726 (2006).
[26] B. Lorenz, F. Yen, M. M. Gospodinov, and C. W. Chu, Phys. Rev. B **71**, 014438 (2005).
[27] C. dela Cruz, F. Yen, B. Lorenz, Y. Q. Wang, Y. Y. Sun, M. M. Gospodinov, and C. W. Chu, Phys. Rev. B **71**, 060407(R) (2005).
[28] J. L. Luo, N. L. Wang, G. T. Liu, D. Wu, X. N. Jing, F. Hu, and T. Xiang, Phys. Rev. Lett. **93**, 187203 (2004).

[29] H. D. Zhou, J. A. Janik, B. W. Vogt, Y. J. Jo, L. Balicas, M. J. Case, C. R. Wiebe, J. C. Denyszyn, J. B. Goodenough, and J. G. Cheng, Phys. Rev. B **74**, 094426 (2006).

[30] L. Ghivelder, I. A. Castillo, M. A. Gusmão, J. A. Alonso, and L. F. Cohen, Phys. Rev. B **60**, 12184 (1999).

[31] J. Park, M. Kang, J. Kim, S. Lee, K.-H. Jang, A. Pirogov, J.-G. Park, C. Lee, S.-H. Park, and H. C. Kim, Phys. Rev. B **79**, 064417 (2009).

[32] A. A. Nugroho, N. Bellido, U. Adem, G. Nénert, Ch. Simon, M. O. Tjia, M. Mostovoy, and T. T. M. Palstra, Phys. Rev. B **75**, 174435 (2007).

[33] P. J. Brown and T. Chatterji, J. Phys. Condens. Matter **18**, 10085 (2006).

[34] S. Harikrishnan, C. M. N. Kumar, H. L. Bhat, S. Elizabeth, U. K. Rößler, K. Dörr, S. Rößler, and S. Wirth, J. Phys. Condens. Matter **20**, 275234 (2008).